A 4-Degree-of-Freedom Parallel Origami Haptic Device for Normal, Shear, and Torsion Feedback

Sophia R. Williams, *Graduate Student Member, IEEE*, Jacob M. Suchoski, Zonghe Chua, *Graduate Student Member, IEEE*, and Allison M. Okamura, *Fellow, IEEE*

***Abstract*—We present a finger-mounted 4-degree-of-freedom (DoF) haptic device created using origami fabrication techniques. The 4-DoF device uses a parallel kinematic mechanism and is capable of delivering normal, shear, and torsional haptic feedback to the fingertip. Traditional methods of robot fabrication are not well suited for designing small robotic devices because it is challenging and expensive to manufacture small, low-friction joints. Our device uses origami manufacturing principles to reduce complexity and device footprint. We characterize the bandwidth, workspace, and force output of the device. The capabilities of the device, particularly the torsion degree of freedom, are demonstrated in a virtual reality scenario. Our results show that the device can deliver haptic feedback in 4 DoFs with an effective operational workspace of 0.64 cm^3 with $\pm 30^\circ$ rotation at every location. When isolated to a single DoF, the maximum force and torque the device can apply in the x-, y-, z-, and θ-directions are $\pm$1.0 N, $\pm$1.25 N, 1.6 N, and $\pm$5 N$\cdot$ mm; the device has an operating bandwidth of 9 Hz.**

***Index Terms*—Haptics and haptic interfaces, kinematics, soft robot materials and design.**

I. Introduction

HAPTICS, the sense of touch, can improve task performance and realism [1], [2]. However, a barrier to making multi-degree-of-freedom haptic devices ubiquitous consumer products is a lack of high-fidelity mechanisms that are simple and affordable. Many commercial haptic devices are desktop-mounted, or "grounded," limiting the movement of the user [3]. Researchers have recently investigated wearable cutaneous devices for the fingertips, which allow users to move unconstrained in their environment and have the potential to reduce cost and encumbrance [4].

Manuscript received September 28, 2021; accepted January 7, 2022. Date of publication January 25, 2022; date of current version February 8, 2022. This letter was recommended for publication by Associate Editor C. Pacchierotti and Editor J. H. Ryu upon evaluation of the reviewers' comments. This work was supported in part by the National Science Foundation under Grants 1812966 and 1830163, in part by the Stanford Robotics Center Fellowship sponsored by FANUC, in part by the Wu Tsai Neurosciences Institute at Stanford University, and in part by the Stanford Bio-X Fellowship. *(Corresponding author: Sophia R. Williams.)*

Sophia R. Williams is with the Electrical Engineering Department, Stanford University, Stanford, CA 94305 USA, and also with Auris Health, Inc., Redwood City, CA 94065 USA (e-mail: sophiarw@stanford.edu).

Jacob M. Suchoski is with the Mechanical Engineering Department, Stanford University, Stanford, CA 94305 USA, and also with Intuitive Surgical, Inc., Sunnyvale, CA 94086-5301 USA (e-mail: jsucho@umich.edu).

Zonghe Chua and Allison M. Okamura are with the Mechanical Engineering Department, Stanford University, Stanford, CA 94305 USA (e-mail: chuazh@stanford.edu; aokamura@stanford.edu).

Digital Object Identifier 10.1109/LRA.2022.3144798

Some fingertip mounted devices are small and stimulate few degrees of freedom (DoF), such as a 2-DoF wearable cutaneous device designed by Girard *et al.* that provides shear feedback in two directions [5]. Futhermore, Schorr *et al.* developed a 3-DoF actuator using a Delta mechanism that mounts to the fingertip and delivers shear and normal forces [6]. Similarly, Leonardis *et al.* designed and fabricated a 3-DoF device that uses both rotational and spherical DoFs [7]. Researchers have also developed 6-DoF wearable cutaneous devices, which are much bulkier than devices with fewer DoFs [8], [9]. In the current literature of wearable fingertip devices, it is apparent that as the the DoFs increase, the device's size and weight increase substantially.

Haptic interaction in the real world, such as object manipulation, is composed of both kinesthetic and cutaneous feedback. Wearable fingertip devices move the grounding forces closer to area where the device is mounted, reducing the required size and complexity of a device but limiting the kinesthetic forces it can apply. However, previous research has shown that cutaneous stimulation alone is sufficient to render virtual objects of different masses, friction, and stiffness [10]. Additionally, it has been shown that as the number of DoFs of the device increases, users use less grip force and rate the haptic feedback as more realistic [11]. As research on wearable devices for the fingertips is still nascent, the most desirable device characteristics, such as number of DoFs, that maximize the trade-off between realism and cost or size are unclear. It is an open question whether the improvement in realism is worth the additional cost and complexity of adding additional DoFs.

Parallel kinematic mechanisms are mechanisms that can achieve large forces and many DoFs with a small form factor. However, manufacturing techniques for creating wearable parallel haptic devices for the fingertip are limited and rely on rigid linkages and mechanisms, which are often expensive, difficult to manufacture at small sizes, and are not easily scalable for production. This is in contrast to origami (foldable) manufacturing techniques, which have recently been explored in haptic applications. Mintchev *et al.* demonstrated the utility of origami robotics in haptics in a 3-DoF origami force feedback device [12]. Their origami device is integrated into a holdable interface that rests in the palm of the user. They demonstrated how the device could be used for virtual reality, teleoperation, and surgical applications. Additionally, Giraud *et al.* created a wearable 3-DoF fingertip origami device for the fingertips that uses an embedded low-profile actuator and weighs only 13 g [13]. However, origami

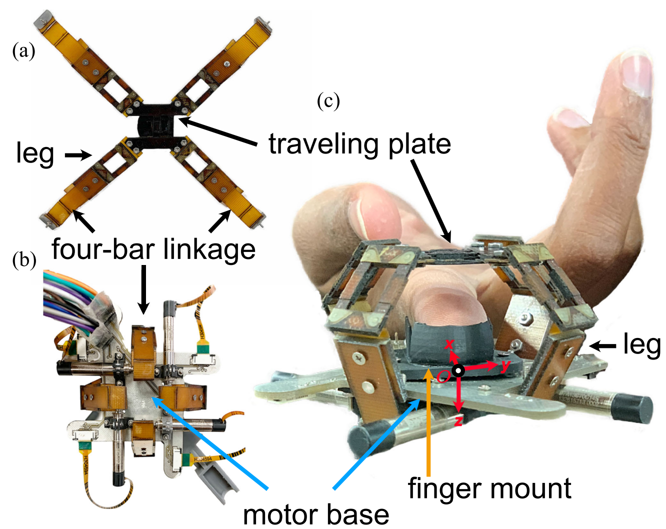

Fig. 1. Different views of the 4-DoF origami cutaneous haptic device, which can apply normal, x- and y-shear, and torsion haptic feedback. The device is a parallel mechanism with 4 legs, where each leg is actuated by its own motor connected to the mechanism using a four-bar linkage. (a) The origami device lays flat with the tactor, the component that contacts the skin of the fingerpad, visible. (b) The motor base. Four bar linkages are attached to each motor shaft using a 3D printed interface. (c) The complete 4-DoF origami cutaneous haptic device, mounted to the index finger of a user. The tactor is mounted to the traveling plate.

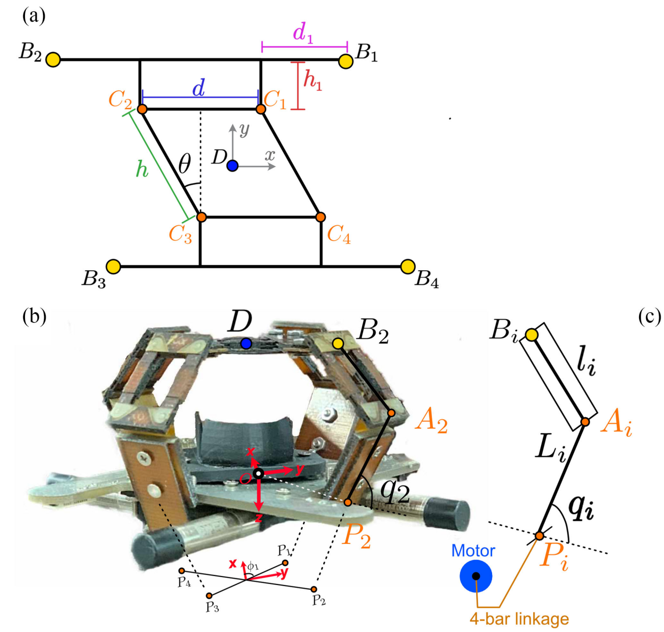

Fig. 2. Diagram to describe relevant kinematic variables. (a) Kinematic variables of traveling plate. (b) Leg 2 projected on origami device. (c) Projection of leg in plane for ease of defining kinematic variables. $\vec{AB_i}$ is a parallelogram for all legs.

manufacturing techniques have not been explored for wearable cutaneous haptic devices with more DoFs.

In this paper, we first discuss the forward kinematics and present the inverse kinematics of a 4-DoF mechanism. Next, we show the design of a 4-DoF cutaneous fingertip device that uses origami fabrication methods. We demonstrate that the haptic device is able to deliver normal, shear and torsion feedback, with up to 1.6 N of force and 8 N-mm of torque. Additionally, we characterize the workspace and bandwidth and demonstrate the device in a virtual reality scenario. The main contribution of this work is a design and manufacturing technique for multi-DoF parallel mechanisms for wearable haptics with compact form factors.

II. Kinematics

The origami assembly is a 4-DoF parallel mechanism comprised of four legs and a traveling plate with a tactor that interfaces with the skin (Fig. 1). In this section, we describe the kinematics of the parallel mechanism, including the kinematic chain (geometry and important parameters), inverse kinematics (IK), and forward kinematics (FK).

A. Kinematic Chain

The kinematic architecture is inspired by a 4-DoF manipulator proposed by Pierrot *et al.* [14]. Each origami leg is composed of two rotational joints followed by a parallelogram (equivalent to a 1-DoF π 4-bar linkage). The parallelogram on each joint provide constraints that confine the shear (x- and y- directions) movement in a plane orthogonal to the z-direction. An additional rotational joint attaches each of the four parallelograms to a corner of the traveling plate. The traveling plate contains another parallelogram, $C_{1\text{-}4}$, where one bar of the parallelogram connects to a tactor. Table I summarizes the performance and parameters of the device.

A schematic detailing the configuration of each leg, the traveling plate, and the kinematic variables is shown in Fig. 2. The task space coordinates of the tactor position, which is defined as the center of the traveling plate, D is designated by x, y, z, and θ. The vector between the origin O and D is, $\overrightarrow{OD} = (x, y, z)^T$. Given the symmetry of the parallel robot, each of the 4 kinematic chains, $i = 1, 2, 3, 4$, has the same geometric representation and each can be analyzed independently. We define the joint angles of the four legs as q_i, $i = 1, 2, 3, 4$.

A_i, B_i, and C_i are the centers of their respective joints and are pictured in Fig. 2. We observe that the magnitude of the vector formed between A_i and B_i must be equal to the link length, l_i:

$$||\overrightarrow{A_iB_i}||^2 = l_i^2. \tag{1}$$

We define the center of each actuated joint, or the joints where the angle is directly controlled, to be $P_i = (x_i, y_i, z_i)^T$. We compute $\overrightarrow{A_iB_i}$ for each leg using the following relationship:

$$\overrightarrow{OP_i} + \overrightarrow{P_iA_i} + \overrightarrow{A_iB_i} + \overrightarrow{B_iC_i} = \overrightarrow{OD} + \overrightarrow{DC_i}. \tag{2}$$

The vector $\overrightarrow{P_iA_i}$ is defined as:

$$\overrightarrow{P_iA_i} = \begin{bmatrix} L\cos\phi_i \cos q_i \\ L\sin\phi_i \cos q_i \\ -L\sin q_i \end{bmatrix}, \tag{3}$$

where ϕ_i is the angle of the linkage with respect to the origin. We define $\phi_1 = \frac{\pi}{4}$, $\phi_2 = \frac{3\pi}{4}$, $\phi_3 = \frac{5\pi}{4}$, $\phi_4 = \frac{7\pi}{4}$, given the placement of the legs with respect to the axes. Additionally,

$\overrightarrow{OP_i} = P_i$. The vectors $\overrightarrow{DB_i}$ for our configuration are:

$$\overrightarrow{DB_1} = \begin{bmatrix} -\frac{1}{2}h\sin\theta + d_1 + \frac{d}{2} \\ \frac{1}{2}h\cos\theta + h_1 \\ 0 \end{bmatrix},$$

$$\overrightarrow{DB_2} = \begin{bmatrix} -\frac{1}{2}h\sin\theta - d_1 - \frac{d}{2} \\ \frac{1}{2}h\cos\theta + h_1 \\ 0 \end{bmatrix}$$

$$\overrightarrow{DB_3} = \begin{bmatrix} \frac{1}{2}h\sin\theta - d_1 - \frac{d}{2} \\ -\frac{1}{2}h\cos\theta - h_1 \\ 0 \end{bmatrix},$$

$$\overrightarrow{DB_4} = \begin{bmatrix} \frac{1}{2}h\sin\theta + d_1 + \frac{d}{2} \\ -\frac{1}{2}h\cos\theta - h_1 \\ 0 \end{bmatrix}$$

Using (1), we derive the following relationship between the joint angles $\vec{q} = (q_1, q_2, q_3, q_4)$ and the task space coordinates x, y, z, and θ, where $\overrightarrow{DB_i}$ is dependent on θ:

$$l_i^2 = \left\| \begin{bmatrix} x \\ y \\ z \end{bmatrix} + \overrightarrow{DB_i} - \begin{bmatrix} L\cos\phi_i\cos q_i \\ L\sin\phi_i\cos q_i \\ -L\sin q_i \end{bmatrix} \right\|^2. \tag{4}$$

B. Inverse Kinematics

The IK of this 4-DoF parallel mechanism were originally presented by Pierrot *et al.* [14]. Solving (4) for q_i, $i = 1, 2, 3, 4$, provides us with the inverse kinematics of the system. For convenience we say that:

$$\begin{bmatrix} X_i \\ Y_i \\ Z_i \end{bmatrix} = \begin{bmatrix} x \\ y \\ z \end{bmatrix} + \overrightarrow{DB_i} \tag{5}$$

We arrange (4) such that it has the form $I_i \sin q_i + J_i \cos q_i + K_i = 0$. We then find the joint angle q_i to be:

$$q_i = 2\arctan\left(\frac{-I_i \pm \sqrt{\Delta}}{K_i - J_i}\right) \tag{6}$$

where $\Delta_i = \sqrt{I_i^2 - K_i^2 + J_i^2}$. Given (5), we find the following values for I_i, J_i, and K_i

$$\begin{bmatrix} I_i \\ J_i \\ K_i \end{bmatrix} = \begin{bmatrix} 2Z_iL_i \\ -2XL_i\cos\phi_i - 2Y_iL_i\sin\phi_i \\ L_i^2 - l_i^2 + X_i^2 + Y_i^2 + Z_i^2 \end{bmatrix}.$$

After computing q_i for $i = 1, 2, 3, 4$, the motor angle is determined by computing the corresponding angle of the 4-bar mechanism connecting the leg to the motor.

C. Forward Kinematics

Nabat proposed solving the FK with an iterative method [15], [16]. The iterative method was presented instead of the direct solution to the FK because the direct solution is non-trivial. To use the iterative method, the current position is updated using the Jacobian, J, as presented in [14], and the change in $\vec{q}$ over time. The current position of the end effector at time t is defined as $\vec{p_t} = [x_t, y_t, z_t, \theta_t]^T$. The end effector position at the previous time step, $t - \Delta t$, is defined as $\vec{p}_{t-\Delta t} = [x_{t-\Delta t}, y_{t-\Delta t}, z_{t-\Delta t}, \theta_{t-\Delta t}]^T$. We define the change in the actuator angles between time steps as, $\dot{\vec{q}} = (\vec{q_t} - \vec{q}_{t-\Delta t})/\Delta t$, where $q_\tau = [q_{\tau,1}, q_{\tau,2}, q_{\tau,3}, q_{\tau,4}]^T$ and $q_{\tau,i}$ is the joint angle at time τ for leg i. The current position $\vec{p_t}$ is calculated given an previous position $\vec{p}_{t-1}$ using the following update rule:

$$\vec{p_t} = \vec{p}_{t-\Delta t} + J\dot{\vec{q}} \tag{7}$$

Alternatively, the FK is solved directly by finding x, y, z, and θ in (1). In this paper, we present the FK solution. We find the solution by subtracting (4) when $i = 1$ from each of (4) where $i = 2, 3, 4$. The resulting three equations are linear and are written as a system of linear equations. Next, Cramer's rule is applied to solve for x, y, and z. The resulting equations describe the position of the end effector, x, y, and z.

$$x = \frac{a_x + b_x\sin\theta + c_x\cos^2\theta + \cos\theta(d_x + e_x\sin\theta)}{2(a_d + b_d\cos\theta + c_d\sin\theta)} \tag{8}$$

$$y = \frac{a_y - b_y\sin\theta + c_y\sin^2\theta + \cos\theta(d_y + e_y\sin\theta)}{2(a_d + b_d\cos\theta + c_d\sin\theta)} \tag{9}$$

$$z = \frac{a_z + b_z\cos\theta + c_z\cos\theta^2 + \sin\theta(d_z + e_z\cos\theta) + f_z\sin^2\theta}{2(a_d + b_d\cos\theta + c_d\sin\theta)} \tag{10}$$

a_n, b_n, c_n, d_n, e_n, and f_n where $n \in \{x, y, z, d\}$ are coefficients described with long equations. Thus, we created Wolfram Mathematica and MATLAB files of the inverse kinematics, which are available on GitHub at https://github.com/sophiarw/4-DoFForwardKinematics. The resulting values of x, y, and z are substituted back into the (4) when $i = 1$, to solve for θ.

The resulting polynomial is an 8th order polynomial with coefficients c_i, $i = 0...8$. We define $s = \tan\frac{\theta}{2}$, such that the polynomial has the following form,

$$c_0 + c_1s + c_2s^2 + c_3s^3 + c_4s^4 + c_5s^5 + c_6s^6 + c_7s^7 + c_8s^8 = 0. \tag{11}$$

The coefficients c_i, $i = 0...8$ are given in the scripts from the GitHub repository described above. The value of s and consequently θ are found using numerical methods, such as Newton's root-finding algorithm. If no solution exists, then none of the solutions are real. If a solution is possible, one pair (2 of 8) of the solutions is real. Some solutions are also not practically achievable given the torque limits of our motors. Additionally, no solution is defined for $\theta_1 = \theta_4$, $\theta_2 = \theta_3$ as the matrices defined by Cramer's rule lose rank.

The indirect iterative FK is still advantageous in some scenarios as it can be calculated very quickly with just a few linear operations. Our direct method requires solving an 8th order polynomial numerically, so may not be suited to real-time control. The iterative FK method assumes one knows the initial end-effector position, which could require a position sensor or additional calibration step. The iterative FK method can also result in drift with any small errors in actuator position, which may be exacerbated in soft or flexible devices. Our direct FK method can be used if the haptic device only has joint angle sensors because our method allows one to determine the haptic device's end effector position given the current joint angles, enabling more precise control in some scenarios.

III. Design and Fabrication

A. Device Components

The 4-DoF origami device is composed of three separate components: the finger mount, the motor base, and the origami assembly (Fig. 1). The *finger mount* orients the user's fingerpad in the device's workspace and grounds the device to the back of the finger. The finger is secured using Velcro straps placed along the intermediate and proximal phalanges. The *motor base* supports the finger mount, origami device, and motors. The motors are 3 V Maxon DC Motor DCX06 M EB SL with a 57:1 gear head a 128-count optical encoder. The origami device weighs 10 g and the motor base weighs 35 g. The entire device fits into a box of 80 mm × 80 mm × 45 mm. The motors are controlled using a Sensoray 826 DAQ running a PID controller for each motor. The desired motor positions are computed and the motors are controlled with 1900 Hz loop frequency. The *origami assembly* kinematics were described in the previous section, and its fabrication is described below. The tactor, which is the end effector of the robotic mechanism that interfaces with the user's skin, is attached to the parallelogram on the traveling plate of the origami assembly. This parallelogram allows for rotation about the z-axis. The bottom of each leg attaches to a 4-bar linkage that is secured to a motor mounted to the bottom side of the motor base (Fig. 1(a) and (b)).

B. Origami Fabrication Methods

The device is manufactured using origami fabrication methods, wherein sheets of material are laser cut, combined in a heat press at 400 psi and 400 °F, and laser cut again to release their final shape. Fiberglass sheets (0.005 in), the same material used in circuit board manufacturing, act as the rigid layers of the robotic structure. Layers of Kapton (13 μm thick), a flexible material able to withstand high heat, are used to allow rotation at the joints. Dupont Pyralux LF0100 25 μm is a dry sheet adhesive that is used to bind together the layers of Kapton and fiberglass. We used the DPSS Lasers Inc. Samurai UV Marking System to laser cut the layers.

The origami fabrication method is used to construct the traveling plate, Fig. 3(a), and four legs, Fig. 3(b), of the origami assembly. All five parallelograms in the origami assembly use four 1 mm dowel pins as pin joints in each of its four corners. The dowel pins go through layers 3-13 of both the traveling plate and legs in order to to constrain the parallelogram to the other layers. The pin joints introduce additional friction to the system but allow us to create the origami assembly using a layered manufacturing approach while still allowing us to achieve 2-DoF rotations in perpendicular planes. An additional benefit of the pin joints is that they have less backlash compared to flexure joints, increasing the rigidity of the parallel bar mechanism. The

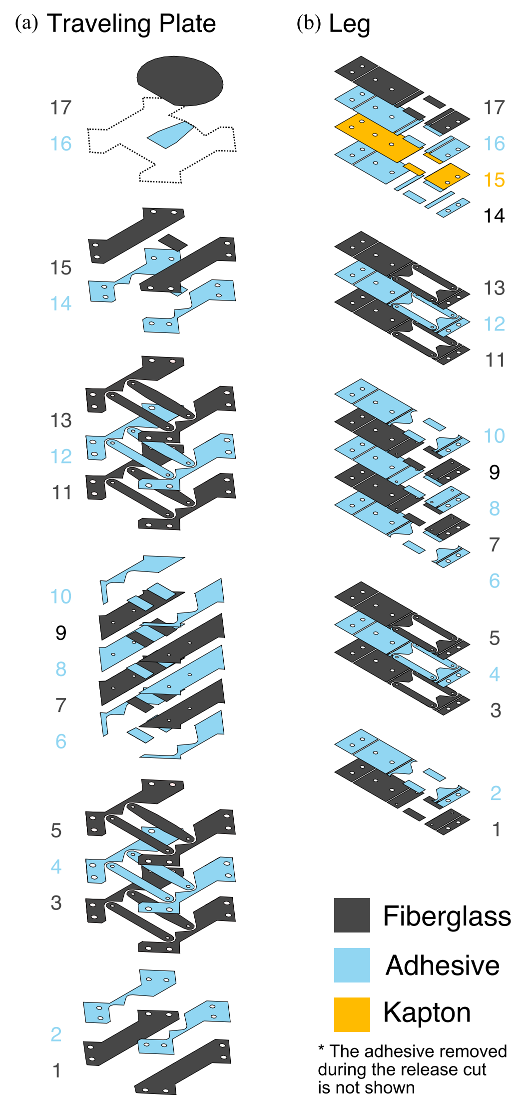

Fig. 3. Fabrication layers for the traveling plate and one origami leg. (a) All 17 layers of the the traveling plate. Four 1 mm pins were used in layers 3-13 to attach the 4-bar linkages to the remaining layers. The pins were added before adhering all layers in a heat press. Layer 17 interfaces directly with the skin of the fingertip. (b) All 17 layers of one origami leg. The Kapton layer (in yellow) is the flexible layer that allows the two links to rotate with respect to one another. The material removed during the release step is not shown in this image.

traveling plate also connects to the tactor shown in Fig. 3(a), Layer 17.

IV. Experiments and Results

A. Bandwidth Testing

Bandwidth testing was performed in each of the four degrees of freedom. The position and orientation of the device end-effector was measured using a ClaroNav MicronTracker, a marker-based optical tracking system.

The position and orientation of the end-effector were measured relative to the base of the device. The z-axis was defined as normal to the plane formed by the motor base, and the x-axis defined such that x-direction movements commanded by the device drivers were approximately parallel. This alignment was

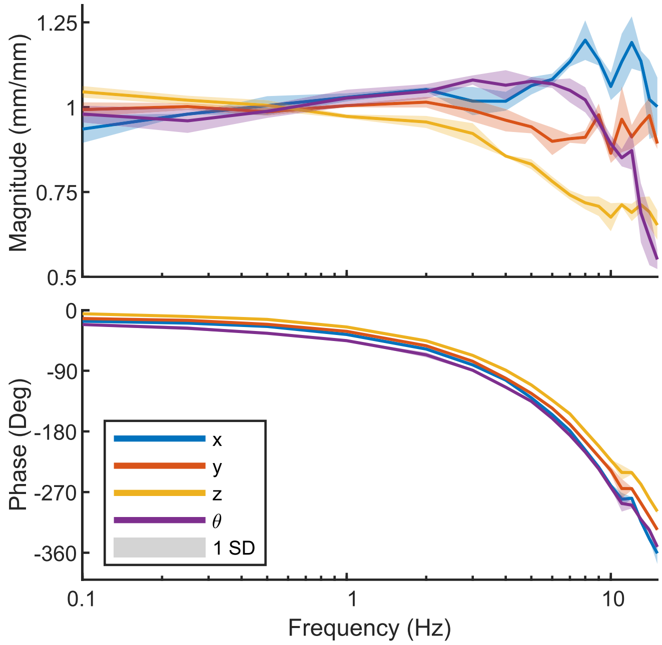

Fig. 4. Bode plot for each of the device DoFs up to 15 Hz. All DoFs have different cutoff frequency and the overall bandwidth of the device is limited by the z-direction, which has a -3 dB cutoff of 9 Hz.

achieved by projecting the first principle direction obtained from the singular value decomposition of data points captured from commanded x-direction movements into the base plane and defining the direction of that vector as the base frame x-axis. Angular displacements about the z-axis were measured directly with respect to the MicronTracker and were projected about the base frame z-axis using the swing-twist decomposition [17], with the base frame z-axis defined as the twist axis.

2 mm amplitude sinusoidal oscillations were commanded in the x, y, and z-directions while 14° amplitude sinusoidal oscillations were commanded in the θ-direction. Three frequency sweeps were conducted, and the magnitudes and phase lags at each frequency were averaged and used to generate the Bode plot shown in Fig. 4. Data points were collected at 0.1, 0.25, 0.5 Hz, and from 1 to 15 Hz in 1 Hz increments.

Each DoFs has a different cutoff frequency, and the overall bandwidth of the device is limited by the z-direction, which has a -3 dB cutoff of 9 Hz. We observed multiple peaks in the amplitude response for all directions and the phase response indicates the system has multiple poles. These results could be due to non-linear friction between layers at the pin joints in the parallelograms on each leg and on the tactor, or by the inherent flexibility of the origami assembly.

B. Device Workspace

Using device kinematics and motor angle limits, the workspace of the device was determined in simulation. The maximum movement in the x, y, z, and θ-directions is $\pm 13, \pm 12$, ± 8 mm, and $\pm 30°$, respectively. However, when the workspace is defined as a cube where every position can achieve minimum 60° total rotation, the reachable workspace is confined

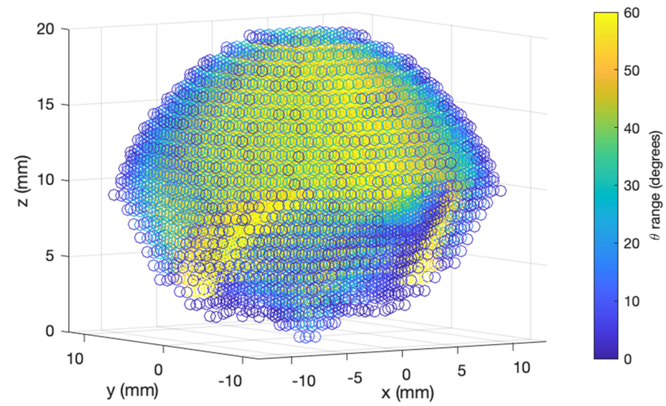

Fig. 5. 3D workspace of the 4-DoF origami device. The kinematic model shows that the workspace spans $\pm$ 13 mm in the x-direction, $\pm$ 12 mm in the y-direction, $\pm$ 8 mm in the z-direction, and $\pm$ 30° in the θ-direction. However, not all θ values are reachable in the workspace. The z-values are negative and start at 0 for ease of visualization.

TABLE I
4-DoF Wearable Haptic Device Technical Specifications

Motor	Maxon DC Motor DCX06M EB SL 3V
Gear Head	Maxon GPX06 A 57:1
Encoder	Maxon ENX 6 OPT, 128 Counts, 2 Channel
Dimensions [mm]	$80 \times 80 \times 45$
Link Lengths [mm]	$L_i = 17.5$, $l_i = 15$, $d_1 = 12.15$, $h_1 = 4.97$, $d = 7.5$, $h = 17.5$ for $i = 1, 2, 3, 4$
Weight [g]	50 g
Max Normal Force [N]	1.6
Max Shear Force [N]	1.5
Max Torque [N·mm]	8

TABLE II
Mean and Standard Deviation of Forces in all DoFs

direction	mean	std
x+ (N)	1.05	0.09
x- (N)	1.06	0.05
y+ (N)	1.25	0.08
y- (N)	1.61	0.08
z+ (N)	1.39	0.13
θ+ (N· mm)	5.6	1.4
θ- (N· mm)	-8.2	0.8

to an $8\text{mm} \times 10\text{mm} \times 8\text{mm}$ cube. Fig. 5 shows the device workspace without constraints. The size of the workspace can be increased by increasing the length of the legs. Consequently, the size of the device and workspace can be modified to accommodate a desired application.

C. Force Measurements

The maximum forces in all directions were measured using an ATI Nano-17 force/torque sensor (ATI Industrial Automation, Apex, NC, USA). The reported values are the maximum force and torque values when the device is constrained in the center of its workspace and is commanded to move in one DoF. The force/torque sensor and the base of the 4-DoF constrained device were mounted so that they could not move relative to one

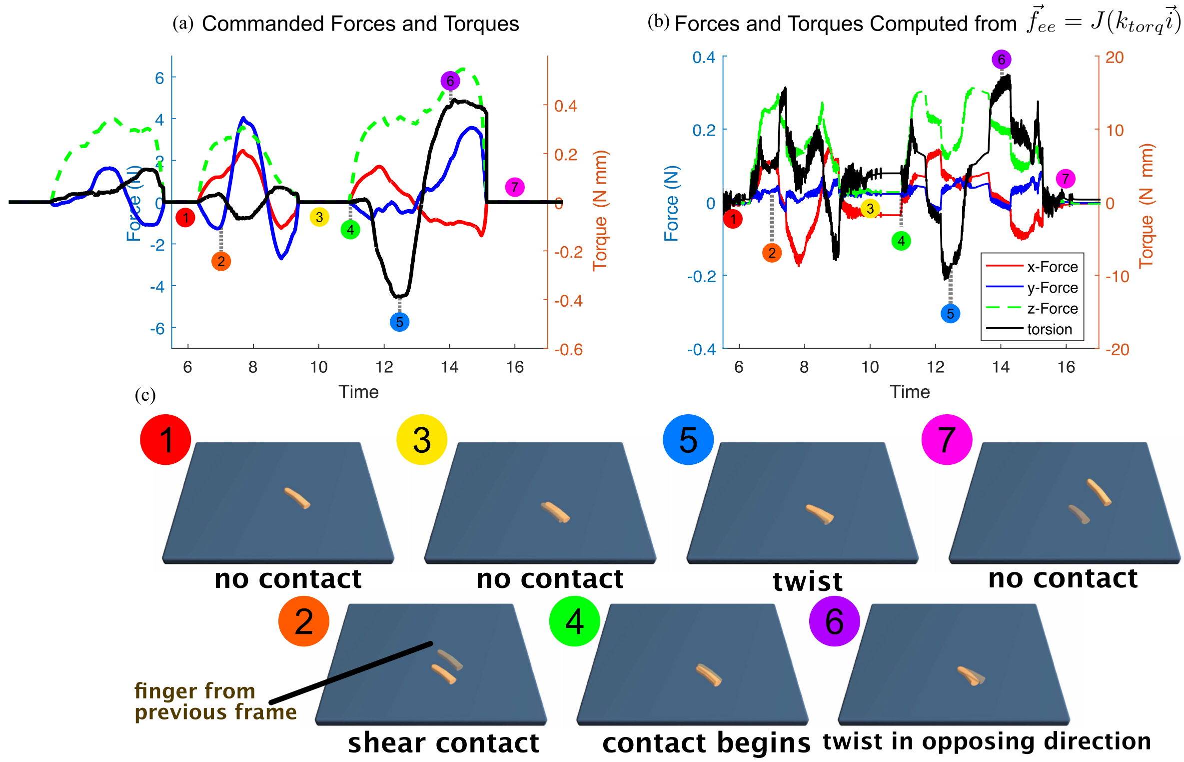

Fig. 6. Demonstration of shear and torsion feedback. (a) Desired force (in N) and torque (in N · mm) over time. From 6 s–10 s, the user creates shear feedback with the object's surface. From 10 s–15 s, the user rotates their finger, creating torsion feedback. (b) Force and torque at the end effector, $\vec{f}_{ee}$, calculated using the Jacobian, J, and the motor torque determined by multiplying the torque constant k_{torq} by the estimated current $\vec{i}$. (c) Snapshots of the finger location in the virtual world during the interaction. Each image shows a semi-transparent rendering of the finger from the proceeding image to indicate how the finger moves. The surface (in blue) is grounded and cannot move within the virtual environment.

another. An alternative traveling plate was used to connect the force/torque sensor securely to the legs of the 4-DoF constrained device. Four repetitions of force measurements were collected in each DoF and the mean and standard deviations are reported in Table II.

The results show that the device can produce $\pm$1-2 N of force in each direction and greater than ± 5 N · mm of torque. We observe that the y-direction produces a larger force than the x-direction. This is expected because the traveling plate is a rectangle, not a square, which results a different moment arm for different legs. We also observe that the positive y-direction forces and θ torques are smaller than the negative y-direction forces and θ torques. This could be due to manufacturing inaccuracies. We are able to deliver forces on the same order of magnitude as prior fingertip devices with rigid links; Schorr *et al.* were able to achieve normal forces of 7.5 N and shear forces of 2.0 N.

V. Virtual Reality Device Demonstration

Here we demonstrate a control strategy in a virtual reality scenario where the device is worn on the index finger of the right hand of the user, and discuss the limitations and benefits of our approach. The CHAI3D framework is used as the rendering environment [20]. CHAI3D uses the god-object algorithm [18] to compute the interaction forces and the friction-cone algorithm to compute the frictional forces [21]. CHAI3D does not include torsion computations for the fingerpad, so we developed a module to compute the torsion shear forces using the soft finger-proxy algorithm (the slip condition was not included) [19]. Software limits were set to confine the workspace to $7\text{mm} \times 9\text{mm} \times 7\text{mm}$. The user's index finger position is detected using a magnetic tracker (3D Guidance trakSTAR, NDI, Waterloo, ON, Canada). During the demonstration, the user sees an avatar of a finger that represents the index finger's location in the virtual environment.

In the demonstration, shown in Fig. 6, the user places their finger on a static virtual surface, resulting in an increase in the z-forces. The virtual surface has a linear stiffness of $500\,\text{N/m}$, static friction of $2.0\,\text{N/m}$, and dynamic friction of $1.8\,\text{N/m}$. The force commanded during the interaction is shown in Fig. 6(a), and the estimated force calculated from motor current and the Jacobian is shown in Fig. 6(b). The interaction of the virtual finger with a virtual surface is depicted in Fig. 6(c). After making contact with the surface, the user moves their finger back and forth primarily in the y-direction. We observe that there is some torsion displayed to the finger but the changing haptic feedback is principally shear feedback. After breaking and making contact with the surface again, the user twists their finger clockwise and then counter-clockwise, primarily activating the torsion degree of freedom.

The control diagram for our system is shown in Fig. 7. The forces computed by CHAI3D based on the user's movement in the virtual environment are converted to a desired position of the

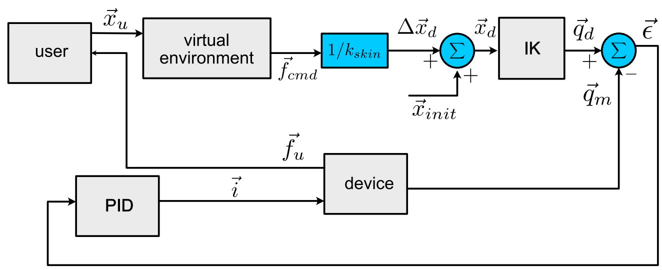

Fig. 7. Control scheme used in the virtual reality demonstration of the origami device. Finger pose $\vec{x}_u$ is measured by a magnetic tracker as the user moves in free space and/or interacts with the virtual surface. The virtual environment computes the desired forces, $\vec{f}_{cmd}$ using the god-proxy algorithm [18] and soft-finger proxy algorithm [19]. During a calibration step we determine the position where the end effector just comes in contact with the user's finger pad $\vec{x}_{init}$. We use estimates of skin stiffness in shear, normal and rotation from the literature to compute the desired change in end effector position Δx_d. The new desired end effector position is calculated $\vec{x}_d$. The inverse kinematics are used to compute the desired actuator angles $\vec{q}_d$. A PID controller uses $\vec{q}_d$ and the measured angular positions of the origami device $\vec{q}_m$ to determine the current $\vec{i}$ to command to the motors. In addition, the interaction between the skin and the device creates an additional force, $\vec{f}_u$, which is also the force felt by the user.

device end effector using an estimate the finger stiffness k_{skin}, as was done in [6]. We use a skin stiffness of 1.58 N/mm in normal and shear [22] 9 N/mm in rotation [19]. The motor current is determined by a PID controller where the error is the difference between the desired and measured position. This control strategy benefits from the faster computation time of the direct IK, but relies on an estimate of the skin's stiffness.

It is challenging to directly measure the forces between the device and the fingertip while a user is interacting with the device. The system behavior is governed by user control of the tactile interaction and their dynamic properties such as skin stiffness and damping. Because we found no existing 4-DoF thin-profile force sensor appropriate for measuring force and torque at the interface between the device and the fingertip, we estimate the force at the end effector using measured motor current. Fig. 6(b) shows the estimated forces delivered to the device end effector, $\vec{f}_{ee}$, computed using the device's Jacobian J, motor torque constant, k_{torque}, (88.92 N $\cdot$ mm/A for our motor torques), and the commanded currents, $\vec{i}$. This estimate is limited in that it does not take into account the torque necessary to overcome friction and other internal forces.

The force estimates show that the force experienced by the device are generally proportional to the commanded input forces, but the commanded forces are higher. This is likely due to inaccuracies in the estimate of finger stiffness, which has been shown to vary across individuals and with finger size [23], and because of variable contact conditions between the device and the fingerpad. The measurement also reveals that the degrees of freedom are not perfectly decoupled. Additionally, given that the commanded torsion is larger than the maximum torque measured at the end effector (Table II) there is torque lost to internal forces. Alternative control strategies, such as impedance, force, or model-based control, may be beneficial to measure and control the forces at the interface between the finger and the origami device.

Overall, the demonstration shows how the 4-DoF origami device provides feedback relevant to common interaction tasks in a virtual environment and how 4 DoFs, not typically available in wearable haptic devices due to size and weight constraints, provide the user with important feedback regarding the virtual object's behavior – namely, the addition of torsion feedback that indicates rotation of the object.

VI. Discussion and Conclusions

The origami parallel mechanism and fabrication techniques presented in this paper introduce design principles that can be used to create wearable devices with high degrees of freedom and low encumbrance. In particular, we are interested in how such devices can be used to investigate fundamental questions about how different degrees of freedom of cutaneous feedback, in particular rotational cues for the fingertip, influence human perception and performance during manipulation tasks. In future work, we plan to investigate user performance as we vary which DoFs are used during manipulation tasks to determine the DoFs that are the most critical for user performance. Additionally, we will investigate how other parallel kinematic structures, with up to 6 DoFs, can be created using origami fabrication methods.

Although the current origami device is able to rotate with with a maximum angle of $\pm 30^\circ$, it is possible that additional rotational displacement may be useful for even more compelling feedback. Researchers have shown that the minimum orientation-change threshold for shear feedback is 14-34° and the number increases to 64° when the individual is engaging in active movement, such as movement that occurs during manipulation tasks [24]. Although these experiments do not directly measure torques or rotational displacements, they indicate that future devices may require larger displacements for users to be able to feel a large range of differential torsional cues. This can be achieved using the device presented in this paper by amplifying the angular displacement using a belt and pulley, as seen in [14], or other mechanisms.

In [8], the researchers found that that rotation cues were perceived with the highest accuracy when stimulating the center of the fingerpad. However, the traveling plates of the current device are constrained to remain flat and the fingermount cannot be adapted to users with different finger curvature or size. Without accurate placement of the device in the center of the finger, the user might have diminished torsion perception. Creating an adjustable tactor or fingermount may improve the overall performance of the device across users.

Acknowledgment

The authors would like to thank Bernie Roth and Dylan Black at Stanford University for their insights regarding mathematical solutions to device kinematics, and also Jamie Paik and Zhenishbek Zhakypov at École polytechnique fédérale de Lausanne for guidance on origami design and fabrication.

REFERENCES

[1] R. P. Khurshid, N. T. Fitter, E. A. Fedalei, and K. J. Kuchenbecker, "Effects of grip-force, contact, and acceleration feedback on a teleoperated pick-and-place task," *IEEE Trans. Haptics*, vol. 10, no. 1, pp. 40–53, Jan.–Mar. 2017.

[2] C. Krogmeier, C. Mousas, and D. Whittinghill, "Human-virtual character interaction: Toward understanding the influence of haptic feedback," *Comput. Animation Virtual Worlds*, vol. 30, no. 3–4, 2019, Art. no. e1883.

[3] G. Cini, A. Frisoli, S. Marcheschi, F. Salsedo, and M. Bergamasco, "A novel fingertip haptic device for display of local contact geometry," in *Proc. World Haptics Conf.*, 2005, pp. 602–605.

[4] C. Pacchierotti, S. Sinclair, M. Solazzi, A. Frisoli, V. Hayward, and D. Prattichizzo, "Wearable haptic systems for the fingertip and the hand: Taxonomy, review, and perspectives," *IEEE Trans. Haptics*, vol. 10, no. 4, pp. 580–600, Oct.–Dec. 2017.

[5] A. Girard, M. Marchal, F. Gosselin, A. Chabrier, F. Louveau, and A. Lécuyer, "HapTip: Displaying haptic shear forces at the fingertips for multi-finger interaction in virtual environments," *Front. ICT*, vol. 3, 2016. [Online]. Available: https://www.frontiersin.org/article/10.3389/fict.2016.00006

[6] S. B. Schorr and A. M. Okamura, "Three-dimensional skin deformation as force substitution: Wearable device design and performance during haptic exploration of virtual environments," *IEEE Trans. Haptics*, vol. 10, no. 3, pp. 418–430, Jul.–Sep. 2017.

[7] D. Leonardis, M. Solazzi, I. Bortone, and A. Frisoli, "A 3-RSR haptic wearable device for rendering fingertip contact forces," *IEEE Trans. Haptics*, vol. 10, no. 3, pp. 305–316, Jul.–Sep. 2017.

[8] E. M. Young and K. J. Kuchenbecker, "Implementation of a 6-DOF parallel continuum manipulator for delivering fingertip tactile cues," *IEEE Trans. Haptics*, vol. 12, no. 3, pp. 295–306, Jul.–Sep. 2019.

[9] Z. F. Quek, S. B. Schorr, I. Nisky, W. R. Provancher, and A. M. Okamura, "Sensory substitution of force and torque using 6-DOF tangential and normal skin deformation feedback," in *Proc. IEEE Int. Conf. Robot. Automat.*, 2015, pp. 264–271.

[10] S. B. Schorr and A. M. Okamura, "Fingertip tactile devices for virtual object manipulation and exploration," in *Proc. CHI Conf. Hum. Factors Comput. Syst.*, 2017, pp. 3115–3119.

[11] J. M. Suchoski, "The role of skin deformation feedback in haptic perception of virtual objects," Ph.D. dissertation, Dept. Mech. Eng., Stanford Univ., Stanford, CA USA, 2019.

[12] S. Mintchev, M. Salerno, A. Cherpillod, S. Scaduto, and J. Paik, "A portable three-degrees-of-freedom force feedback origami robot for human-robot interactions," *Nature Mach. Intell.*, vol. 1, no. 12, pp. 584–593, 2019.

[13] F. H. Giraud, S. Joshi, and J. Paik, "Haptigami: A fingertip haptic interface with vibrotactile and 3-DOF cutaneous force feedback," *IEEE Trans. Haptics*, to be published, doi: 10.1109/TOH.2021.3104216.

[14] F. Pierrot, V. Nabat, O. Company, S. Krut, and P. Poignet, "Optimal design of a 4-DOF parallel manipulator: From academia to industry," *IEEE Trans. Robot.*, vol. 25, no. 2, pp. 213–224, Apr. 2009.

[15] V. Nabat, "Robots parallèles à nacelle articulée, du concept à la solution industrielle pour le pick-andplace," Ph.D. dissertation, Univ. Montpellier II-Sciences et Techniques du Languedoc, Montpellier, France, 2007.

[16] D. E. Whitney, "Resolved motion rate control of manipulators and human prostheses," *IEEE Trans. Man- Mach. Syst.*, vol. 10, no. 2, pp. 47–53, Jun. 1969.

[17] P. Dobrowolski, "Swing-twist decomposition in clifford algebra," *CoRR*, vol. abs/1506.05481, 2015. [Online]. Available: http://arxiv.org/abs/1506.05481

[18] C. Zilles and J. K. Salisbury, "A constraint-based god-object method for haptic display," *ASME Haptic Interfaces Virt. Environ. Teleoperator Syst.*, vol. 1, no. 1, pp. 149–150, 1994.

[19] F. Barbagli, A. Frisoli, K. Salisbury, and M. Bergamasco, "Simulating human fingers: A soft finger proxy model and algorithm," in *Proc. IEEE Int. Symp. Haptic Interfaces Virt. Environ. Teleoperator Syst.*, 2004, pp. 9–17.

[20] F. Conti *et al.*, "The CHAI libraries," in *Proc. Eurohaptics*, Dublin, Ireland, 2003, pp. 496–500.

[21] W. S. Harwin and N. Melder, "Improved haptic rendering for multi-finger manipulation using friction cone based god-objects," in *Proc. Eurohaptics Conf.*, 2002, pp. 82–85.

[22] B. T. Gleeson, S. K. Horschel, and W. R. Provancher, "Perception of direction for applied tangential skin displacement: Effects of speed, displacement, and repetition," *IEEE Trans. Haptics*, vol. 3, no. 3, pp. 177–188, Jul.–Sep. 2010.

[23] S. Sasai, Y.-X. Zhen, T. Suetake, Y. Tanita, S. Omata, and H. Tagami, "Palpation of the skin with a robot finger: An attempt to measure skin stiffness with a probe loaded with a newly developed tactile vibration sensor and displacement sensor," *Skin Res. Technol.*, vol. 5, no. 4, pp. 237–246, 1999.

[24] M. P. Vitello, M. O. Ernst, and M. Fritschi, "An instance of tactile suppression: Active exploration impairs tactile sensitivity for the direction of lateral movement," in *Proc. Eurohaptics Conf.*, 2006, pp. 351–355.